BIOCHEMISTRY
including biophysical chemistry & molecular biology

Article

pubs.acs.org/biochemistry

Time-Resolved Infrared Detection of the Proton and Protein Dynamics during Photosynthetic Oxygen Evolution

Takumi Noguchi,*[,†,‡] Hiroyuki Suzuki,[‡] Masaya Tsuno,[†,‡] Miwa Sugiura,[§,∥] and Chihiro Kato[⊥]

[†]Division of Material Science, Graduate School of Science, Nagoya University, Furo-cho, Chikusa-ku, Nagoya 464-8602, Japan
[‡]Institute of Materials Science, University of Tsukuba, Tsukuba, Ibaraki 305-8573, Japan
[§]Cell-Free Science and Technology Research Center, Ehime University, Matsuyama, Ehime 790-8577, Japan
[∥]PRESTO, Japan Science and Technology Agency (JST), 4-1-8, Honcho, Kawauchi, Saitama 332-0012, Japan
[⊥]Kanagawa Industrial Technology Center, Ebina, Kanagawa 243-0435, Japan

Supporting Information

ABSTRACT: Photosynthetic oxygen evolution by plants and cyanobacteria is performed by water oxidation at the Mn_4CaO_5 cluster in photosystem II. The reaction is known to proceed via a light-driven cycle of five intermediates called S_i states (i = 0−4). However, the detailed reaction processes during the intermediate transitions remain unresolved. In this study, we have directly detected the proton and protein dynamics during the oxygen-evolving reactions using time-resolved infrared spectroscopy. The time courses of the absorption changes at 1400 and 2500 cm^{-1}, which represent the reactions and/or interaction changes of carboxylate groups and the changes in proton polarizability of strong hydrogen bonds, respectively, were monitored upon flash illumination. The results provided experimental evidence that during the $S_3 \rightarrow S_0$ transition, drastic proton rearrangement, most likely reflecting the release of a proton from the catalytic site, takes place to form a transient state before the oxidation of the Mn_4CaO_5 cluster that leads to O_2 formation. Early proton movement was also detected during the $S_2 \rightarrow S_3$ transition. These observations reveal the common mechanism in which proton release facilitates the transfer of an electron from the Mn_4CaO_5 cluster in the S_2 and S_3 states that already accumulate oxidizing equivalents. In addition, relatively slow rearrangement of carboxylate groups was detected in the $S_0 \rightarrow S_1$ transition, which could contribute to the stabilization of the S_1 state. This study demonstrates that time-resolved infrared detection is a powerful method for elucidating the detailed molecular mechanism of photosynthetic oxygen evolution by pursuing the reactions of substrate and amino acid residues during the S-state transitions.

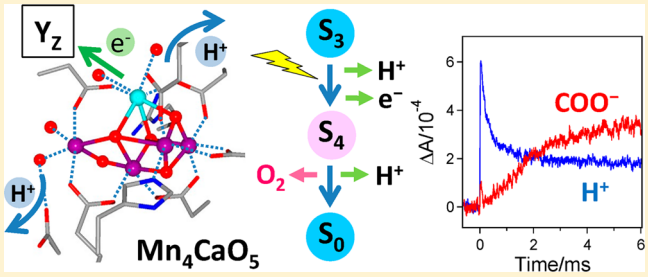

In oxygenic photosynthesis performed by plants and cyanobacteria, solar energy is converted to chemical energy by utilizing water as an ultimate electron donor to reduce CO_2. Molecular oxygen released as a byproduct of the water oxidation is the source of the oxygen atmosphere on which we depend and an ozone layer to protect life from harmful UV light. Thus, photosynthetic oxygen evolution is one of the most significant biological processes that are essential for sustenance of the environment and life on earth.

The oxygen-evolving reaction takes place in photosystem II (PSII) protein complexes embedded in thylakoid membranes.[1−5] Upon illumination on PSII, an electron is ejected from the singlet excited state of the monomeric chlorophyll Chl_{D1} and transferred to the pheophytin electron acceptor, the primary quinone electron acceptor Q_A, and then the secondary quinone electron acceptor Q_B. On the electron donor side, the radical cation of the chlorophyll dimer P680 is produced immediately after charge separation, and it oxidizes Y_Z (D1-Tyr161) and then the oxygen-evolving center (OEC), which is the catalytic site of oxygen evolution. The OEC consists of a Mn_4CaO_5 cluster as a core structure and surrounding amino acid residues providing ligands to the Mn and Ca ions (six carboxylates and one imidazole from the D1 and CP43 subunits) and forming a hydrogen bond network (Figure 1A).[6−9] The recent X-ray crystallographic study at 1.9 Å resolution by Umena et al.[8] resolved the detailed structure of the Mn_4CaO_5 cluster together with four water ligands (only oxygen atoms) as candidates of substrate water (Figure 1A).

As for the reaction mechanism of oxygen evolution, it has been known that water oxidation proceeds via a light-driven cycle (S-state cycle or Kok cycle) of five intermediates called S_i states (i = 0−4).[10,11] Upon illumination of successive flashes, each flash advances the S_i state (i = 0−3) to the next S_{i+1} state, while the transient S_4 state is relaxed to the S_0 state, releasing molecular oxygen (Figure 1B). Because the S_1 state is the most

Received: March 1, 2012
Revised: March 26, 2012
Published: March 29, 2012

dx.doi.org/10.1021/bi300294n | Biochemistry 2012, 51, 3205−3214

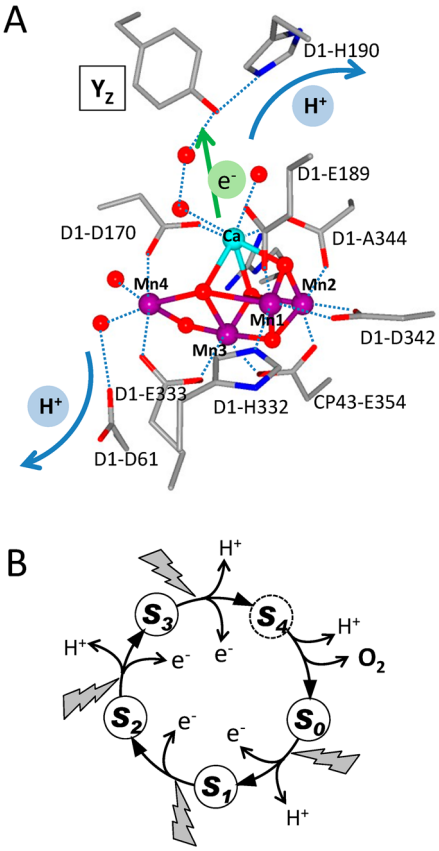

Figure 1. (A) Structure around Y_Z and the OEC in photosystem II, which was deduced from the X-ray crystallographic structure at 1.9 Å resolution (PDB entry 3ARC[8]). Red spheres represent oxygen atoms of water molecules and the Mn_4CaO_5 cluster. Possible proton transfer pathways[8] are shown as blue arrows. (B) Light-driven S-state cycle of photosynthetic oxygen evolution. Upon flash illumination, states S_0–S_3 proceed to states S_1–S_4, respectively. The S_4 state is a transient intermediate that relaxes to the S_0 state, releasing molecular oxygen. Protons are released during the $S_0 \rightarrow S_1$, $S_2 \rightarrow S_3$, and $S_3 \rightarrow S_0$ transitions with a 1:1:2 stoichiometry.[50,62,63]

stable in the dark, oxygen is released upon the third flash and then every four flashes.

To fully understand the oxygen evolution mechanism, it is essential to monitor the reactions of the OEC during individual S-state transitions in a time-dependent manner. In particular, elucidation of the structure and reaction of the enigmatic transient S_4 state formed immediately before the formation of O_2 is crucial to understanding the mechanism of O–O bond formation. The presence of the S_4 state has been proposed in the Kok cycle,[11] but its identity has long been debated.[1−5,12,13] The hint of the S_4 state or its precursor was found in a "lag phase" observed before a slow phase ($t_{1/2}$ > 1 ms) upon the third flash in UV absorption and O_2 evolution measurements.[14−19] Rappaport et al.[16] interpreted this phase ($t_{1/2}$ = 30 μs) as reflecting the release of a proton from the OEC electrostatically triggered by a positive charge generated by the formation of $Y_Z^{\bullet}$. More recently, Haumann et al.[20] found using time-resolved X-ray absorption spectroscopy (XAS) that during the lag phase of ∼250 μs no change in the oxidation state of the Mn ions took place and hence concluded that the formation of the S_4 state (later denoted as S_3^n)[12] is a deprotonation process rather than an electron transfer reaction. To elucidate further details of the reaction mechanism during the $S_3 \rightarrow S_0$ transition as well as proton-coupled electron transfer in the other transitions, another spectroscopic method that can directly monitor the reactions of substrates, protons, and amino acid groups is required.

In this study, we have applied time-resolved infrared (IR) absorption spectroscopy to the analysis of the reaction process during the S-state transitions in the OEC. IR spectroscopy, especially light-induced Fourier transform infrared (FTIR) difference spectroscopy,[22−25] has been used to study the structure and reactions of the OEC, including the Mn core moiety,[21,26] amino acid residues,[27−31] protein main chains,[32] and water molecules,[33,34] via detection of structural changes between the relaxed S_i states (i = 0–3). Here, we have performed time-resolved IR measurements during the S-state transitions at 1400 and 2500 cm^{-1}, which represent the vibrations of carboxylate groups and strong hydrogen bonds with high proton polarizability, respectively. The results revealed the multistep movements of protons and proteins during the photosynthetic oxygen evolution, especially during the $S_3 \rightarrow S_4 \rightarrow S_0$ transition.

MATERIALS AND METHODS

Samples. The PS II core complexes from thermophilic cyanobacterium *Thermosynechococcus elongatus* strain 43-H, in which the carboxyl terminus of the CP43 subunit was genetically histidine-tagged, were purified using Ni^{2+} affinity column chromatography as described previously.[35] The O_2 evolution activity of the core sample was 2500 μM O_2 (mg of Chl)$^{-1}$ h^{-1} with 0.5 mM 2,6-DCBQ as an electron acceptor at 25 °C. The complexes were suspended in a 10 mM Mes-NaOH (pH 6.0) buffer containing 5 mM NaCl, 5 mM $CaCl_2$, and 0.06% *n*-dodecyl β-D-maltoside and concentrated to ∼4.5 mg of Chl/mL using Microcon-100 (Amicon). An aliquot of the sample suspension (7 μL) was mixed with 1 μL of 100 mM potassium ferricyanide and dried on a CaF_2 plate (25 mm × 25 mm) under N_2 gas in an oval shape (6 mm × 9 mm). The sample was hydrated by placing 2 μL of a 20% (v/v) glycerol/water solution in a sealed IR cell without touching the sample.[36] Note that at the relative humidity determined by the 20% glycerol/water solution, the PSII sample is hydrated enough to retain high efficiencies in all the S-state transitions.[36] The sample temperature was kept at 10 ± 1 °C by circulating cold water through a copper holder.

Time-Resolved IR Measurements. Time-resolved IR measurements were performed using a transient IR system with a dispersive-type IR spectrometer.[37,38] The sample was excited by the second harmonic (532 nm) of a Q-switched Nd:YAG laser (Spectron Laser Systems, model SL801) [pulse width, ∼10 ns (fwhm); power, ∼6 mJ/pulse], which was fired by triggers to a flash lamp. The beam diameter was expanded to ∼1 cm to illuminate the whole sample area. Monitoring light from a ceramic IR source (JASCO) (∼1500 K), from which visible light was removed by a Ge filter (>4000 cm^{-1} cut), was dispersed using an IR grating monochromator (modified model IR-700 from JASCO) after passing through the sample and focused onto a photoconductive MCT detector (EG&G Judson, model J15D14). The change in the intensity of the IR light induced by photoreaction was extracted by a high-pass filter circuit (>1.0 Hz) followed by a low-noise preamplifier (NF Electronics Instruments, model KGA-17377; DC ∼ 1 MHz bandwidth). The signal was then amplified using a second amplifier (Stanford Research Systems, model SR560) and recorded on a 1 GHz digital oscilloscope (LeCroy, model

dx.doi.org/10.1021/bi300294n | *Biochemistry* 2012, 51, 3205–3214

LC534A). The bandwidth of the second amplifier was 10 kHz − 1 Hz to reduce higher- and lower-frequency noise. The rise time of a signal was ~25 μs, which was determined by this high-frequency filter. Ten successive pulses with 500 ms intervals were illuminated on a PSII sample, and the signals were recorded from −10 to 90 ms upon each pulse with 4 μs/point. The monochromator was fixed to 1400 or 2500 cm^{-1} with a spectral resolution of 16 cm^{-1}. After one measurement with a train of 10 flashes, the sample was adapted to the dark for 1 h on ice and used for another measurement. It has been shown that this dark adaptation relaxes all the S_i states (i = 0, 2, and 3) to the S_1 state under these sample conditions.[36] Note that the S_0 state is oxidized to the S_1 state in the dark in the presence of ferricyanide, and hence, preflashes are not necessary.[36] The results of 12 measurements using three samples (four measurements for each sample) and those of seven measurements using three samples (one to four measurements for each sample) were averaged for final data at 1400 and 2500 cm^{-1}, respectively.

Data analyses, including the simulation of oscillation patterns and curve fitting of the time courses, were performed using IGOR Pro (Wavemetrics Inc.). In the kinetic analysis, curve fitting was performed in the time range from the initial peak time (24−32 μs) to 0.5, 2.0, 6.0, and 3.0 ms for the $S_1 \rightarrow S_2$, $S_2 \rightarrow S_3$, $S_3 \rightarrow S_0$, and $S_0 \rightarrow S_1$ transitions, respectively. These long time limits were determined by searching appropriate times to provide reasonable time constants. The errors of the time constants were estimated by changing the long time limits in the fitting analysis and changing the miss factors to calculate the traces of the pure S-state transitions. In the latter case, miss factors were changed within the error range of an average miss factor or assuming that the miss of the $S_3 \rightarrow S_0$ transition is 2 times greater than the misses of other transitions.[39]

RESULTS

Time-resolved IR measurements of the OEC reactions were performed at two different wavenumbers, 1400 and 2500 cm^{-1}. Previous flash-induced FTIR difference spectra of the S-state cycle (Figure S1 of the Supporting Information)[33,40,41] demonstrated that bands around 1400 cm^{-1}, which were assigned to the symmetric stretching vibrations of carboxylate groups,[27,42,43] exhibited negative intensities at the first and second flashes and positive intensities at the third and fourth flashes, indicating that carboxylate groups drastically change their structures and interactions during water oxidation reactions. Around 2500 cm^{-1}, broad continuum bands due to the vibrations of OH or NH groups in strong hydrogen bonds with high proton polarizability[44] have been observed (Figure S1 of the Supporting Information).[33] The broad feature and the frequencies that are much lower than those of the usual NH/OH vibrations originate from the AH···B ↔ A^-···H^+B equilibrium of a strong hydrogen bond.[44] The strongest intensity was detected at the third flash, while the first flash provided the lowest intensity. Thus, via detection of the absorption changes at 1400 and 2500 cm^{-1}, the dynamics of carboxylate groups and protons in hydrogen bonds can be monitored during the S-state transitions of the OEC. On the other hand, the reduction of quinone electron acceptors, Q_A and Q_B, on the electron acceptor side shows almost no contribution at these wavenumbers.[45−48] The electron transfer reactions on the electron acceptor side can be monitored at 2036 cm^{-1}, where the intense CN stretching band of ferrocyanide appears[27] by reduction of ferricyanide as an exogenous electron acceptor, and at 1480 cm^{-1}, where the strong CO/CC stretching bands of semiquinone anions of Q_A^- and Q_B^- appear.[45−48] The results of the analysis of the acceptor side reactions are presented as Supporting Information.

Figure 2A shows the time course of ΔA at 1400 cm^{-1} upon the first to tenth flash illumination on the PSII core complexes.

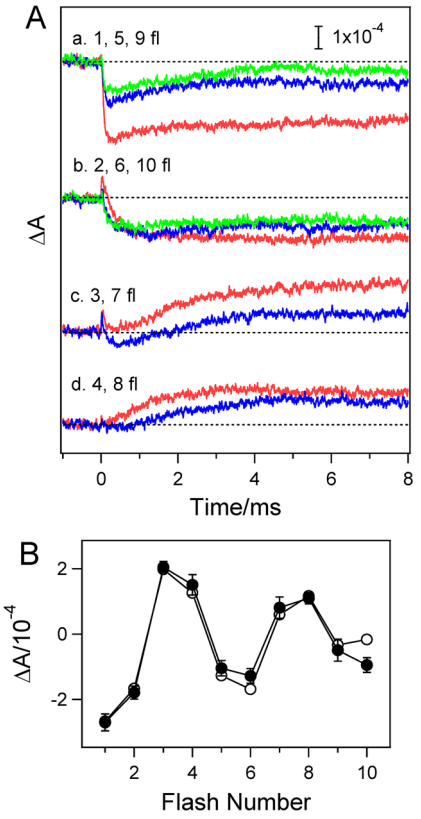

Figure 2. (A) Time course of ΔA at 1400 cm^{-1} of the PSII core complexes upon first- to tenth-flash illumination: (a) first, fifth, and ninth flashes, (b) second, sixth, and tenth flashes, (c) third and seventh flashes, and (d) fourth and eighth flashes. The traces from the first to fourth, fifth to eighth, and ninth to tenth flashes are colored red, blue, and green, respectively. (B) Flash number dependence of ΔA at 1400 cm^{-1} at 6 ms [average of the data between 5.7 and 6.3 ms (●)] and a fitting pattern providing an average miss factor of 11% (○). The error bars are standard deviations of the values obtained from individual measurements.

The first, fifth, and ninth flashes (Figure 2A, a) induced a fast decrease in intensity, while the second, sixth, and tenth flashes (Figure 2A, b) exhibited a small increase in the magnitude of the signal at the beginning followed by a decay to a negative intensity. The time course at the third and seventh flashes (Figure 2A, c) showed a specific shape of curves; there was a fast decay from a small positive intensity followed by a slow sigmoidal rise. The fourth and eighth flashes (Figure 2A, d) also showed a relatively slow rise but without an initial fast decay. The observed similar shapes of curves among the traces at every four flashes indicate that there is a period four oscillation typical of the S-state cycle. This is explicitly shown in the flash number dependence of the ΔA value at 6 ms, at which the reactions in the OEC were virtually completed [Figure 2B (●)]. This oscillation pattern was simulated with a parameter of a single miss factor with the assumption that there is no double hit because of the use of ~10 ns pulses and the fact that all the

dx.doi.org/10.1021/bi300294n | Biochemistry 2012, 51, 3205−3214

centers are poised on the S_1 state before the first flash (see Materials and Methods). The simulated pattern provided a miss factor of 11 ± 3% [Figure 2B (○)]. The observed oscillation pattern and the relative amplitudes at individual flashes are virtually identical to our previous results from flash-induced FTIR difference measurements (Figure S1 of the Supporting Information),[33,36] which accumulated a signal for 10 s after flash illumination.

Figure 3A shows the time course of ΔA at 2500 cm^{-1} upon the first to tenth flashes. At this wavenumber, all the curves

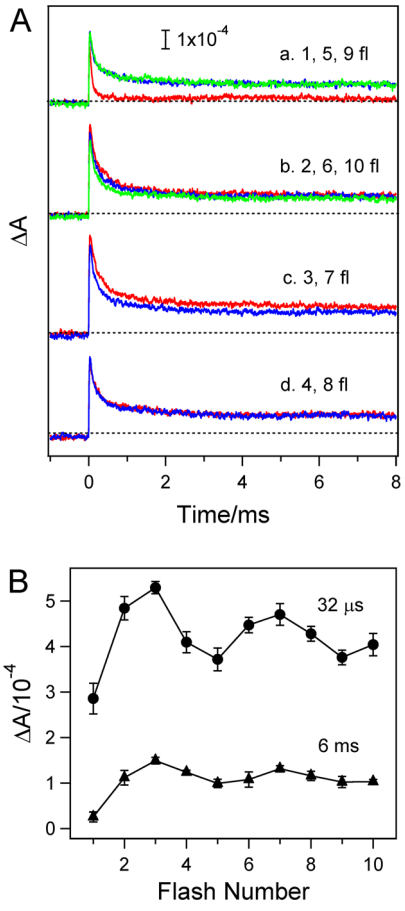

Figure 3. (A) Time course of ΔA at 2500 cm^{-1} of the PSII core complexes upon the first to tenth illumination flashes: (a) first, fifth, and ninth flashes, (b) second, sixth, and tenth flashes, (c) third and seventh flashes, and (d) fourth and eighth flashes. The traces from the first to fourth, fifth to eighth, and ninth to tenth flashes are colored red, blue, and green, respectively. (B) Flash number dependence of ΔA at 2500 cm^{-1} at 32 μs (●) and 6 ms [average of the data between 5.7 and 6.3 ms (▲)]. The error bars are standard deviations of the values obtained from individual measurements.

showed initial positive intensities followed by decays to constant values in the microsecond to millisecond region. The ΔA values of the initial positive maxima at 32 μs [the time to give maxima was basically determined by the time resolution of the present system (see Materials and Methods)] and those of the relaxed levels at 6 ms both showed a period four oscillation, indicative of monitoring the S-state cycle in the OEC. The observation that ΔA values are always positive in all the traces even at the relaxed levels (e.g., at 6 ms), which is in sharp contrast to the traces at 1400 cm^{-1} (Figure 2), indicates that the origin of the IR signals at 2500 cm^{-1} includes hydrogen bonds with high proton polarizability produced by protons released from substrate water.

Using a miss factor of 11%, the corrected time courses of the pure S-state transitions ($S_1 \rightarrow S_2$, $S_2 \rightarrow S_3$, $S_3 \rightarrow S_0$, and $S_0 \rightarrow S_1$) at 1400 and 2500 cm^{-1} were calculated (Figures 4–7;

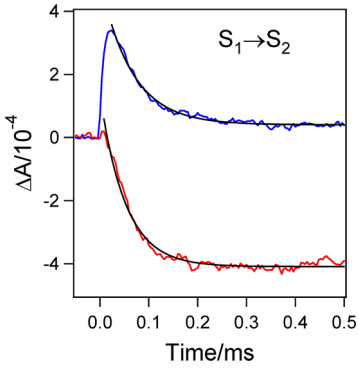

Figure 4. Corrected time course of ΔA at 1400 cm^{-1} (red) and 2500 cm^{-1} (blue) in the $S_1 \rightarrow S_2$ transition. Fitting curves assuming single-exponential functions are shown as black lines.

Figure S4 of the Supporting Information for the comparison in the same time range of 0–4 ms; see the Supporting Information for the calculation procedure). In the $S_1 \rightarrow S_2$ transition (Figure 4), both of the decay curves at 1400 cm^{-1} (red line) and 2500 cm^{-1} (blue line) were well fit with single-exponential functions (black lines) with relatively fast rates of 50 ± 10 and 65 ± 10 μs, respectively.

As for the $S_2 \rightarrow S_3$ transition (Figure 5A), the decay curves at 1400 cm^{-1} (red line) and 2500 cm^{-1} (blue line) could be fit with single-exponential functions with similar rates of 350 ± 30 and 310 ± 50 μs, respectively. However, the fitting was not satisfactory for the trace at 2500 cm^{-1}; clearly, there is another fast phase (Figure 5A, blue line, and Figure 5B, a). Thus, further fitting was performed using a double-exponential function (Figure 5B, b), which provided a residual (Figure 5B, d) much smaller than that from a single-exponential function (Figure 5B, c). The obtained time constants were 70 ± 10 and 460 ± 50 μs (the relative amplitudes were 0.38 and 0.62, respectively). Similar time constants of 80 ± 10 and 470 ± 50 μs were also obtained by assuming a consecutive reaction (see the Supporting Information for a fitting function). Even in the decay curve of 1400 cm^{-1}, there seems to be another phase with a silent intensity in the early time region of <100 μs (Figure 5A, red line). Indeed, when fitting was performed using a function of a consecutive reaction (see the Supporting Information), the first silent phase of 75 ± 20 μs followed by a slower phase of 320 ± 30 μs was obtained. However, the residual by this fitting was not much different from that by the single-exponential fitting (data not shown). We need a further careful study to draw a clear conclusion about the fast phase in the time course of 1400 cm^{-1}.

The ΔA trace at 1400 cm^{-1} in the $S_3 \rightarrow S_0$ transition showed a rather complex shape (Figure 6A, red line). There is a fast decay in the early time region (<100 μs) followed by a slow, sigmoidal rise in the millisecond region. This sigmoidal rise suggests the presence of an early phase with a silent intensity (Figure 6B). This basic shape of the curve was unchanged when the corrected $S_3 \rightarrow S_0$ trace was calculated using miss factors of 14 and 8%, which are the highest and lowest values, respectively, within the error range (11 ± 3%) (Figure S5A

dx.doi.org/10.1021/bi300294n | Biochemistry 2012, 51, 3205–3214

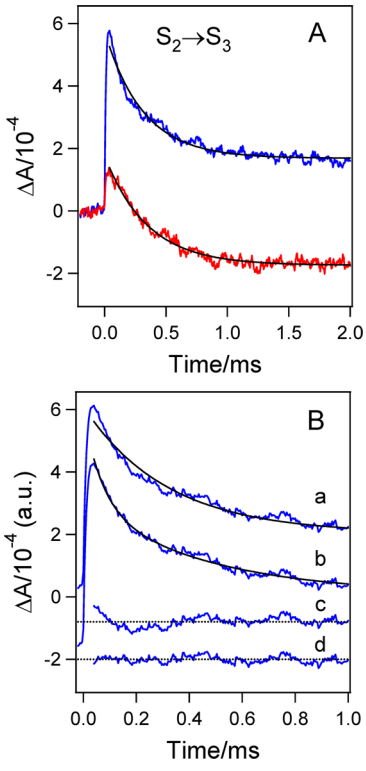

Figure 5. (A) Corrected time course of ΔA at 1400 cm^{-1} (red) and 2500 cm^{-1} (blue) in the $S_2 \rightarrow S_3$ transition. Fitting curves assuming exponential functions are shown in black lines. (B) Comparison between the fitting curves assuming single-exponential (a) and double-exponential (b) functions (black). The residuals of the curve fitting in parts a and b are shown as parts c and d, respectively. Dotted lines in parts c and d express zero lines.

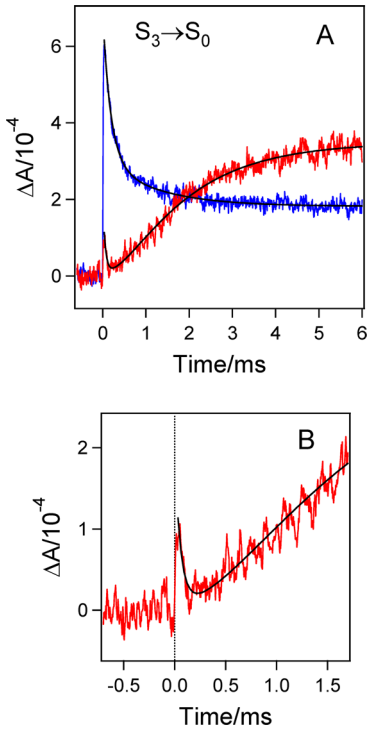

Figure 6. (A) Corrected time course of ΔA at 1400 cm^{-1} (red) and 2500 cm^{-1} (blue) in the $S_3 \rightarrow S_0$ transition. The fitting curves are shown as back lines. A consecutive reaction was assumed for the 2500 cm^{-1} trace, and a consecutive reaction, including a first silent phase with an additional single-exponential phase (for the initial decay), was assumed for the 1400 cm^{-1} trace (for the fitting functions, see the Supporting Information). (B) Expanded view of the early time region of the trace at 1400 cm^{-1} (red) with a fitting curve (black).

of the Supporting Information, traces b and c, respectively), and using a miss factor set with a 2 times greater value in the $S_3 \rightarrow S_0$ transition than in other transitions, keeping the average miss factor of 11% (i.e., 17.6% for the $S_3 \rightarrow S_0$ transition and 8.8% for others) (Figure S5A of the Supporting Information, trace d). The latter miss factor set was selected because it has been suggested that the miss of the $S_3 \rightarrow S_0$ transition is significantly larger than the misses of other transitions.[39] Fitting analysis was performed assuming a consecutive reaction, in which the first reaction is a silent phase and the second reaction provides a positive ΔA value, with an additional single-exponential decay in the early time region (see the Supporting Information for a fitting function). The result showed time constants of 60 ± 15 μs (relative amplitude of 0.35) for the initial fast decay, 550 ± 50 μs (0) for the silent phase, and 1550 ± 150 μs (0.65) for the slow rise. The expanded view of the early time region (Figure 6B) shows that at the beginning of the sigmoidal rise, there seems to be a "lag time" of 200−400 μs, on which a fast decay component is superimposed.

The decay curve at 2500 cm^{-1} of the $S_3 \rightarrow S_0$ transition (Figure 6A, blue line) clearly showed double phases with relatively fast and slow decays. This decay curve was well fit with a consecutive reaction with time constants of 190 ± 15 μs (relative amplitude of 0.78) and 1200 ± 150 μs (0.22) (see the Supporting Information for a fitting function). Fitting using double-exponential functions also provided very similar time constants.

In contrast to the $S_3 \rightarrow S_0$ transition, the $S_0 \rightarrow S_1$ transition showed relatively simple traces at both 1400 and 2500 cm^{-1} (Figure 7, red and blue lines, respectively). Fitting of the decay curve of 2500 cm^{-1} using double-exponential functions

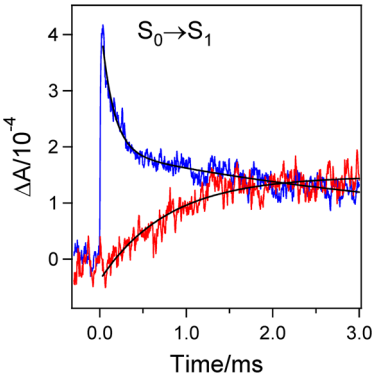

Figure 7. Corrected time course of ΔA at 1400 cm^{-1} (red) and 2500 cm^{-1} (blue) in the $S_0 \rightarrow S_1$ transition. Fitting curves assuming single- and double-exponential functions for 1400 and 2500 cm^{-1}, respectively, are colored black.

provided a major phase with a time constant of 130 ± 10 μs (relative amplitude of 0.59) together with a rather slow phase of 1−4 ms (0.41). On the other hand, the trace of 1400 cm^{-1} showed a simple rise that can be fit with a single-exponential function with a time constant of 800 ± 100 μs. It is noticeable that no sigmoidal shape was observed in the initial rise, suggestive of the absence of the silent phase in contrast to the $S_3 \rightarrow S_0$ transitions. This shape of the simple rise was basically

dx.doi.org/10.1021/bi300294n | *Biochemistry* 2012, 51, 3205−3214

unchanged when different miss factors [14 and 8% for all the transitions and a miss factor set of 17.6% for the $S_3 \rightarrow S_0$ transition and 8.8% for other transitions (see above)] were used in calculation of the corrected $S_0 \rightarrow S_1$ trace (Figure S5B of the Supporting Information).

DISCUSSION

Understanding the coupling of electron and proton transfer reactions together with the relevant protein dynamics is crucial for unraveling the water oxidation mechanism in photosynthesis. We used transient IR spectroscopy to monitor the proton and protein reactions during the S-state transitions of the OEC by detecting absorbance changes at 1400 and 2500 cm^{-1}. Strong bands around 1400 cm^{-1} arising from the symmetric stretching vibrations of carboxylate groups[27,42,43] are characteristic of flash-induced FTIR difference spectra of the S-state cycle (Figure S1 of the Supporting Information),[40,41] reflecting the strong coupling of the Mn_4CaO_5 cluster with carboxylate groups, which are ligands to the Mn/Ca ions or indirectly coupled through a hydrogen bond network (Figure 1A). Thus, the time-dependent absorbance changes at this wavenumber reveal the perturbations of the carboxylate ligands triggered by the redox change of the Mn ions[28−30] or those of carboxylate groups in a hydrogen bond network around the Mn_4CaO_5 cluster,[49] including the protonation−deprotonation reactions in proton pathways. On the other hand, the absorbance changes at 2500 cm^{-1}, where broad features due to high proton polarizability of strong hydrogen bonds appear (Figure S1),[33,44] reveal the movements or changes of interaction of protons in a hydrogen bond network within the protein as well as the release of protons into the bulk. Such high proton polarizability of hydrogen bonds is essential in all proton transfer processes in proteins.[44] Thus, monitoring the time-dependent changes of the proton polarizability of hydrogen bonds provides information about proton transfer in S-state transitions.

Time-resolved IR changes at 1400 cm^{-1} (Figures 4−7 and Figure S4 of the Supporting Information, red lines) exhibited significantly different traces depending on the S-state transitions. The $S_1 \rightarrow S_2$ (Figure 4) and $S_2 \rightarrow S_3$ (Figure 5) transitions showed single-exponential decays in contrast to a single-exponential rise in the $S_0 \rightarrow S_1$ transition (Figure 7). A rather complex behavior was observed in the $S_3 \rightarrow S_0$ transition: a fast decay followed by a slow, sigmoidal rise (Figure 6). The initial amplitudes immediately after flash excitation were almost zero in the $S_1 \rightarrow S_2$ and $S_0 \rightarrow S_1$ transitions, while small positive signals were observed in the $S_2 \rightarrow S_3$ and $S_3 \rightarrow S_0$ transitions, indicating that the formation of $Y_Z^{\bullet}$ induces small structural perturbations of nearby carboxylate groups in the S_2 and S_3 states. This observation reflects a slightly different protein environment around Y_Z depending on the S states.

In contrast to the transients at 1400 cm^{-1}, the initial ΔA amplitudes at 2500 cm^{-1} always showed strong positive values in all the S-state transitions (Figures 4−7 and Figure S4 of the Supporting Information, blue lines). This finding indicates that oxidation of Y_Z creates a strong hydrogen bond(s) with high proton poralizability in the protein, suggesting that a proton released from oxidized Y_Z remains in the nearby protein moiety, possibly as a proton of D1-His190 hydrogen bonding to $Y_Z^{\bullet}$.[5,13] The observation of a clear period four oscillation pattern of the initial amplitudes of the flash-induced IR changes [Figure 3B (●)] indicates that the structure of the hydrogen bond network around Y_Z is different from one S state to another, reflecting the presence of strong structural coupling between Y_Z and the Mn_4CaO_5 cluster. All the traces at 2500 cm^{-1} exhibited only decay components, suggesting that the proton polarization near $Y_Z^{\bullet}$ relaxes during the S-state transition. However, even after relaxation, positive signals were left in all the S-state transitions, although the amplitude was rather small in the $S_1 \rightarrow S_2$ transition (Figure S4 of the Supporting Information). These positive intensities originate from both the rearrangements of hydrogen bonds around the OEC and protons released from the OEC to the bulk. In the latter case, released protons protonate buffer molecules[50] or protonatable groups on the surface of the protein[40] and generate strong hydrogen bonds with high proton polarizability. Thus, the period four oscillation in the flash number dependence of ΔA at 6 ms [Figure 3B (▲)] may also involve the contributions of protons released from the OEC. Indeed, this oscillation pattern, i.e., the minima at the first, fifth, and ninth flashes and the maxima at tthe hird and seventh flashes, is very similar to the flash number dependence of the release of protons from the OEC monitored using FTIR signals of Mes buffer for the same *T. elongatus* core complexes.[50] In the latter study, the number of protons released was estimated to be 0.8−1.0, 0.2−0.3, 0.9−1.2, and 1.5−1.6 for $S_0 \rightarrow S_1$, $S_1 \rightarrow S_2$, $S_2 \rightarrow S_3$, and $S_3 \rightarrow S_0$ transitions, respectively, reflecting the proton release pattern of 1:0:1:2 from substrate water with additional contributions of protonation−deprotonation reactions of nearby amino acid residues. The observation that only the first flash, which provides the pure $S_1 \rightarrow S_2$ transition, exhibited a very low intensity at 6 ms (Figure 3A) may reflect the small number of protons released in this transition. The higher intensities at the fifth and ninth flashes can be attributed to the mixing of other transitions due to miss hits (11 ± 3%).

Barry et al.[51] previously reported the results of time-resolved IR signals at 1483 cm^{-1} induced by excitation of PSII preparations by a train of short flashes. These data, however, cannot be reconciled for several reasons with previous FTIR studies and the results of time-resolved measurements obtained by other spectroscopies. (1) Always positive ΔA values were observed at 1483 cm^{-1} after relaxation of the S-state transitions (e.g., at 10 ms) in contrast to previous FTIR spectra of the S-state cycle exhibiting almost no intensity at 1483 cm^{-1} (Figure S1 of the Supporting Information).[27−29,40−43] Thus, these positive ΔA values cannot originate from reactions of the OEC. (2) High negative intensities were observed immediately after flash illumination and attributed to Q_A^- formation.[51] However, the most prominent feature of the Q_A^-/Q_A FTIR difference spectrum is a strong *positive* band around 1480 cm^{-1} due to the CO/CC vibrations of the semiquinone anion.[45−47] Thus, the observation is inconsistent with the Q_A^- assignment. Our time-resolved IR measurement at 1480 cm^{-1} convincingly showed a positive intensity due to the formation of Q_A^- and a decay phase with a τ of 300−500 μs that can be attributed to the transfer of an electron from Q_A^- to Q_B (Figure S3 of the Supporting Information). (3) Although the intensity at 1483 cm^{-1} was assigned to the His vibration in ref 51, no strong His vibration has been detected at this position in previous His isotope-edited FTIR measurements of the OEC.[52,53] (4) The positive intensity at 1483 cm^{-1} in OEC-inactivated PSII has been attributed to $Y_Z^{\bullet}$.[51] However, the previous $Y_Z^{\bullet}/Y_Z$ FTIR difference spectrum presented by Berthomieu et al.[54] showed no intense peak at this position. We also reproduced a $Y_Z^{\bullet}/Y_Z$ spectrum that is very similar to that of Berthomieu et al.[54] (data

Table 1. Time Constants (microseconds) of the ΔA Changes at 1400 and 2500 cm^{-1} in the S-State Transitions

	$S_1 \rightarrow S_2$	$S_2 \rightarrow S_3$	$S_3 \rightarrow S_0$	$S_0 \rightarrow S_1$
1400 cm^{-1}	50 ± 10 (d)[a]	350 ± 30 (d)	60 ± 15 (d, 0.35)	800 ± 100 (r)
			550 ± 50 (s, 0)	
			1550 ± 150 (r, 0.65)	
2500 cm^{-1}	65 ± 10 (d)	70 ± 10 (d, 0.38)	190 ± 15 (d, 0.78)	130 ± 10 (d, 0.59)
		460 ± 50 (d, 0.62)	1200 ± 150 (d, 0.22)	1000−4000 (d, 0.41)

[a] d, r, and s in parentheses indicate decay, rise, and silent components, respectively. Also, figures in parentheses indicate the relative amplitudes of individual phases.

not shown). (5) The time constants reported by Barry et al.[51] are inconsistent with previous data obtained by other methods like UV absorption,[14,16,19,55−57] EPR,[58,59] and XAS.[20] For example, they reported a major phase (68%) with a rate of 1100 μs at the first flash, and that (78%) with a rate of 770 μs at the second flash. In addition, a faster phase (22%) at the second flash showed a rate (58 μs) faster than that (32%) at the first flash (93 μs). These observations are totally different from the kinetics of the S-state transitions so far reported (see below). The considerations of points 1−5 strongly suggest that the previous transient IR data of Barry et al.[51] are mostly due to unknown origins.

The time constants estimated in this study by fitting procedures of the corrected traces of the S-state transitions (Figures 4−7) are summarized in Table 1 and Figure 8. Single-exponential decays at 1400 and 2500 cm^{-1} in the $S_1 \rightarrow S_2$ transition (Figure 4) provided similar time constants in the range of 50−70 μs. These relatively short transition rates of <100 μs are in good agreement with the rate of this transition reported in previous studies.[14,16,19,20,55−59] This observation is consistent with the view that the rearrangements of protons in strong hydrogen bonds and those of carboxylate groups are directly coupled with the transfer of an electron from the Mn_4CaO_5 cluster to $Y_Z^{\bullet}$. In particular, the similar time constants between the decay at 2500 cm^{-1} and the Mn oxidation in the $S_1 \rightarrow S_2$ transition examined by XAS measurements[20] indicate that a proton shift is not only coupled but also concerted with the electron transfer in this transition.

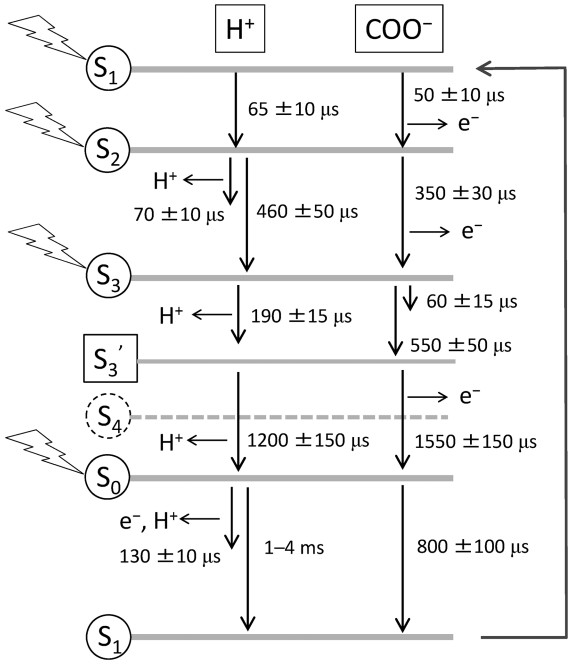

Figure 8. Kinetic scheme of the movements of protons and carboxylate groups during the S-state cycle.

As for the $S_2 \rightarrow S_3$ transition, previous EPR, UV absorption, and XAS measurements showed single-exponential kinetics with a time constant of 100−400 μs.[14,16,19,20,55−59] This value is in agreement with the time constants of 300−400 μs obtained from our transient IR data of 1400 and 2500 cm^{-1} (Figure 5A), assuming single-exponential decays. However, the decay curve of 2500 cm^{-1} clearly consists of two phases; double-exponential fitting provided a fast phase ($\tau \sim 70$ μs) along with a slow phase ($\tau \sim 460$ μs). Because this slow phase and the ~350 μs decay of 1400 cm^{-1} seem to correspond to the transfer of an electron from the Mn_4CaO_5 cluster to $Y_Z^{\bullet}$, the fast phase of 70 μs may reflect rearrangement of protons in hydrogen bonds in proteins or even the release of a proton to the bulk that takes place faster than the electron transfer. This result suggests that proton transfer precedes electron transfer in the $S_2 \rightarrow S_3$ transition. Although the trace of 1400 cm^{-1} is also consistent with the presence of a lag phase of <100 μs, a definitive conclusion was not reached. Further studies are necessary to identify a distinct intermediate during the $S_2 \rightarrow S_3$ transition.

In the $S_3 \rightarrow S_0$ transition where O_2 formation and subsequent release take place, a distinct intermediate has been identified as a lag phase in UV absorption[16,17] and XAS[20] measurements. Haumann et al.[20] recognized this intermediate as the S_4 state but later denoted it as S_3^n.[12] In this paper, we denote this intermediate as S_3' [the expression $(Y_Z^{\bullet}S_3)'$ was used by Rappaport et al.[17]] to distinguish it from the S_4 state that should have a catalytic center oxidized by $Y_Z^{\bullet}$. It has been proposed that during the transition to this intermediate, a deprotonation reaction takes place from the OEC without changes in the redox states of the Mn_4CaO_5 cluster and $Y_Z^{\bullet}$.[16,20] In this time-resolved IR measurement, we indeed detected the movement of a proton during this lag phase. The change in ΔA at 2500 cm^{-1} due to high proton polarizability exhibits a fast phase of ~190 μs (Figure 6A), which is in good agreement with the ~200 μs lag phase reported previously,[20] followed by a ~1200 μs slow phase that may correspond to the electron transfer phase concomitant with O_2 release.[15,58,59] In addition, the change in ΔA at 1400 cm^{-1} due to the carboxylate vibrations showed a clear sigmoidal shape in the rise of a slow phase ($\tau \sim 1550$ μs) that may correspond to the 1200 μs phase at 2500 cm^{-1}, suggesting the presence of a lag phase with a silent IR intensity before the electron transfer. The fitting analysis assuming a consecutive reaction showed that this silent phase has a time constant of ~550 μs, which is greater than the time constant of the fast phase at 2500 cm^{-1} (~190 μs). Thus, it is possible that after the release of the proton from the $Y_Z^{\bullet}S_3$ state, further protein relaxation occurs to form the S_3' state. Another notable observation is that there is an additional fast decay phase ($\tau \sim 60$ μs) in carboxylate movements before the

dx.doi.org/10.1021/bi300294n | Biochemistry 2012, 51, 3205−3214

silent phase. This fast phase is even faster than the proton transfer phase (~190 μs) at 2500 cm^{-1} mentioned above, and hence, it could be related to the protein rearrangement upon formation of $Y_Z^{\bullet}$, which has been reported to take place in 30–40 μs.[5,13,60,61]

The $S_0 \rightarrow S_1$ transition is characterized by a rather strange behavior in protons of strong hydrogen bonds and carboxylate groups. The trace at 2500 cm^{-1} (Figure 7, blue line) showed a major phase with a relatively fast rate ($\tau \sim 130$ μs), whereas the trace at 1400 cm^{-1} (Figure 7, red line) exhibited a single-exponential rise with a much slower rate ($\tau \sim 800$ μs). A slow minor decay at 2500 cm^{-1} ($\tau = 1–4$ ms) could correspond to this slow phase at 1400 cm^{-1}. Because other spectroscopic methods (UV absorption, EPR, and XAS) have estimated relatively fast transfer (<250 μs)[16,20,55−59] of an electron from the Mn_4CaO_5 cluster to $Y_Z^{\bullet}$ in this transition, it appears reasonable to assign the 130 μs phase of 2500 cm^{-1} to the electron transfer coupled with a proton transfer reaction. It is worth noting that although previous measurements mostly exhibited a time constant of the $S_0 \rightarrow S_1$ transition shorter than or comparable to that of the $S_1 \rightarrow S_2$ transition,[20,55−59] our value of 130 μs is more consistent with that by Rappaport et al.,[16] who showed a longer time constant of the $S_0 \rightarrow S_1$ transition (250 μs) than that of the $S_1 \rightarrow S_2$ transition (55 μs). The much slower carboxylate change (~800 μs) was unexpected. The absence of a phase of carboxylate movements corresponding to the electron transfer suggests that the carboxylate groups with vibrations around 1400 cm^{-1} and influenced by the $S_0 \rightarrow S_1$ transition are not direct ligands to the Mn ion oxidized in this transition. Rather, these carboxylate groups may be indirectly coupled to the Mn_4CaO_5 cluster and reflect the relaxation of the protein conformation after electron transfer.

CONCLUSION

Our time-resolved IR measurement directly monitored the multistep reactions of proteins and protons during photosynthetic oxygen evolution. The results provided experimental evidence that in the $S_3 \rightarrow S_0$ transition, drastic proton rearrangements take place during the lag phase that precedes the transfer of an electron from the Mn_4CaO_5 cluster to $Y_Z^{\bullet}$. This observation strongly supports the view that upon $Y_Z^{\bullet}S_3$ formation one proton is released either directly from substrate water or from an amino acid residue near the catalytic center to form a transient intermediate, S_3', followed by the oxidation of substrate and O–O bond formation. In addition, we have detected the movement of a proton in an early stage during the $S_2 \rightarrow S_3$ transition, which may reflect a proton release reaction coupled with electron transfer.[12] These early deprotonation processes may facilitate the oxidation of the OEC that accumulates oxidizing equivalents in the S_2 and S_3 states by lowering its redox potential.[12,16,20] We have also observed a relatively slow carboxylate movement during the $S_0 \rightarrow S_1$ transition after the proton and probably electron transfer reactions. This protein relaxation process could contribute to the stabilization of the S_1 state relative to other S states. This study demonstrates that time-resolved IR spectroscopy is a powerful method for directly monitoring the proton and protein dynamics during intermediate transitions in photosynthetic oxygen evolution. Further studies to detect water molecules and different amino acid residues will significantly contribute to our understanding of the oxygen evolution mechanism.

ASSOCIATED CONTENT

Supporting Information

Analysis of the acceptor side reactions, the calculation procedure of the time courses of pure S-state transitions, fitting functions including a consecutive reaction, FTIR difference spectra of the S-state cycle, time course of ΔA at 2036 and 1480 cm^{-1}, corrected time course of ΔA at 1400 and 2500 cm^{-1} of the four S-state transitions in the same time range (<4 ms), and corrected time course of ΔA at 1400 cm^{-1} in the $S_3 \rightarrow S_0$ and $S_0 \rightarrow S_1$ transitions calculated using different miss factors. This material is available free of charge via the Internet at http://pubs.acs.org.

AUTHOR INFORMATION

Corresponding Author

*Phone: +81-52-789-2881. Fax: +81-52-789-2883. E-mail: tnoguchi@bio.phys.nagoya-u.ac.jp.

Funding

This study was supported by the Grants-in-Aid for Scientific Research from the Ministry of Education, Culture, Sports, Science and Technology (21370063, 23108706, and 23657099 to T.N.) and the JST-PRESTO program (4018 to M.S.).

Notes

The authors declare no competing financial interest.

ABBREVIATIONS

EPR, electron paramagnetic resonance; FTIR, Fourier transform infrared; IR, infrared; Mes, 2-(*N*-morpholino)-ethanesulfonic acid; OEC, oxygen-evolving center; PSII, photosystem II; XAS, X-ray absorption spectroscopy; PDB, Protein Data Bank.

REFERENCES

(1) Debus, R. J. (1992) The manganese and calcium ions of photosynthetic oxygen evolution. *Biochim. Biophys. Acta 1102*, 269–352.

(2) Hillier, W., and Messinger, J. (2005) Mechanism of photosynthetic oxygen production. In *Photosystem II: The Light-Driven Water:Plastoquinone Oxidoreductase* (Wydrzynski, T., and Satoh, K., Eds.) pp 567–608, Springer, Dordrecht, The Netherlands.

(3) McEvoy, J. P., and Brudvig, G. W. (2006) Water-splitting chemistry of photosystem II. *Chem. Rev. 106*, 4455–4483.

(4) Messinger, J., Noguchi, T., and Yano, J. (2011) Photosynthetic O_2 Evolution. In *Molecular Solar Fuels* (Wydrzynski, T., and Hillier, W., Eds.) pp 163–207, Chapter 7, Royal Society of Chemistry, Cambridge, U.K.

(5) Renger, G. (2012) Photosynthetic water splitting: Apparatus and mechanism. In *Photosynthesis: Plastid Biology, Energy Conversion and Carbon Assimilation* (Eaton-Rye, J. J., Tripathy, B. C., and Sharkey, T. D., Eds.) pp 359–414, Springer, Dordrecht, The Netherlands.

(6) Ferreira, K. N., Iverson, T. M., Maghlaoui, K., Barber, J., and Iwata, S. (2004) Architecture of the photosynthetic oxygen-evolving center. *Science 303*, 1831–1838.

(7) Guskov, A., Kern, J., Gabdulkhakov, A., Broser, M., Zouni, A., and Saenger, W. (2009) Cyanobacterial photosystem II at 2.9-Å resolution and the role of quinones, lipids, channels and chloride. *Nat. Struct. Mol. Biol. 16*, 334–342.

(8) Umena, Y., Kawakami, K., Shen, J. R., and Kamiya, N. (2011) Crystal structure of oxygen-evolving photosystem II at a resolution of 1.9 Å. *Nature 473*, 55–60.

(9) Yano, J., Kern, J., Sauer, K., Latimer, M. J., Pushkar, Y., Biesiadka, J., Loll, B., Saenger, W., Messinger, J., Zouni, A., and Yachandra, V. K. (2006) Where water is oxidized to dioxygen: Structure of the photosynthetic Mn_4Ca cluster. *Science 314*, 821–825.

(10) Joliot, P., Barbieri, G., and Chabaud, R. (1969) Model of the System II photochemical centers. *Photochem. Photobiol. 10*, 309−329.
(11) Kok, B., Forbush, B., and McGloin, M. (1970) Cooperation of charges in photosynthetic O_2 evolution-I. A linear four step mechanism. *Photochem. Photobiol. 11*, 457−475.
(12) Dau, H., and Haumann, M. (2008) The manganese complex of photosystem II in its reaction cycle: Basic framework and possible realization at the atomic level. *Coord. Chem. Rev. 252*, 273−295.
(13) Renger, G. (2007) Oxidative photosynthetic water splitting: Energetics, kinetics and mechanism. *Photosynth. Res. 92*, 407−425.
(14) Koike, H., Hanssum, B., Inoue, Y., and Renger, G. (1987) Temperature dependence of S-state transition in a thermophilic cyanobacterium, *Synechococcus vulcanus* Copeland measured by absorption changes in the ultraviolet region. *Biochim. Biophys. Acta 893*, 524−533.
(15) Razeghifard, M. R., and Pace, R. J. (1999) EPR kinetic studies of oxygen release in thylakoids and PSII membranes: A kinetic intermediate in the S_3 to S_0 transition. *Biochemistry 38*, 1252−1257.
(16) Rappaport, F., Blanchard-Desce, M., and Lavergne, J. (1994) Kinetics of electron-transfer and electrochromic change during the redox transitions of the photosynthetic oxygen-evolving complex. *Biochim. Biophys. Acta 1184*, 178−192.
(17) Rappaport, F., Ishida, N., Sugiura, M., and Boussac, A. (2011) Ca^{2+} determines the entropy changes associated with the formation of transition states during water oxidation by Photosystem II. *Energy Environ. Sci. 4*, 2520−2524.
(18) Haumann, M., Bogershausen, O., Cherepanov, D., Ahlbrink, R., and Junge, W. (1997) Photosynthetic oxygen evolution: H/D isotope effects and the coupling between electron and proton transfer during the redox reactions at the oxidizing side of Photosystem II. *Photosynth. Res. 51*, 193−208.
(19) Gerencser, L., and Dau, H. (2010) Water oxidation by photosystem II: H_2O-D_2O exchange and the influence of pH support formation of an intermediate by removal of a proton before dioxygen creation. *Biochemistry 49*, 10098−10106.
(20) Haumann, M., Liebisch, P., Müller, C., Barra, M., Grabolle, M., and Dau, H. (2005) Photosynthetic O_2 formation tracked by time-resolved X-ray experiments. *Science 310*, 1019−1021.
(21) Chu, H.-A., Hillier, W., Law, N. A., and Babcock, G. T. (2001) Vibrational spectroscopy of the oxygen-evolving complex and of manganese model compounds. *Biochim. Biophys. Acta 1503*, 69−82.
(22) Noguchi, T., and Berthomieu, C. (2005) Molecular analysis by vibrational spectroscopy. In *Photosystem II: The Light-Driven Water:-Plastoquinone Oxidoreductase* (Wydrzynski, T., and Satoh, K., Eds.) pp 367−387, Springer, Dordrecht, The Netherlands.
(23) Noguchi, T. (2007) Light-induced FTIR difference spectroscopy as a powerful tool toward understanding the molecular mechanism of photosynthetic oxygen evolution. *Photosynth. Res. 91*, 59−69.
(24) Noguchi, T. (2008) Fourier transform infrared analysis of the photosynthetic oxygen-evolving center. *Coord. Chem. Rev. 252*, 336−346.
(25) Debus, R. J. (2008) Protein ligation of the photosynthetic oxygen-evolving center. *Coord. Chem. Rev. 252*, 244−258.
(26) Chu, H.-A., Sackett, H., and Babcock, G. T. (2000) Identification of a Mn-O-Mn cluster vibrational mode of the oxygen-evolving complex in photosystem II by low-frequency FTIR spectroscopy. *Biochemistry 39*, 14371−14376.
(27) Noguchi, T., Ono, T., and Inoue, Y. (1995) Direct detection of a carboxylate bridge between Mn and Ca^{2+} in the photosynthetic oxygen-evolving center by means of Fourier transform infrared spectroscopy. *Biochim. Biophys. Acta 1228*, 189−200.
(28) Chu, H.-A., Hillier, W., and Debus, R. J. (2004) Evidence that the C-terminus of the D1 polypeptide of photosystem II is ligated to the manganese ion that undergoes oxidation during the S_1 to S_2 transition: An isotope-edited FTIR study. *Biochemistry 43*, 3152−3166.
(29) Service, R. J., Yano, J., McConnell, I., Hwang, H. J., Niks, D., Hille, R., Wydrzynski, T., Burnap, R. L., Hillier, W., and Debus, R. J. (2011) Participation of glutamate-354 of the CP43 polypeptide in the ligation of manganese and the binding of substrate water in photosystem II. *Biochemistry 50*, 63−81.
(30) Shimada, Y., Suzuki, H., Tsuchiya, T., Tomo, T., Noguchi, T., and Mimuro, M. (2009) Effect of a single amino acid substitution of the 43 kDa chlorophyll-protein on the oxygen-evolving reaction of the cyanobacterium *Synechocystis* sp. PCC 6803: Analysis of the Glu354Gln mutation. *Biochemistry 48*, 6095−6103.
(31) Shimada, Y., Suzuki, H., Tsuchiya, T., Mimuro, M., and Noguchi, T. (2011) Structural coupling of an arginine side chain with the oxygen evolving Mn_4Ca cluster in photosynstem II as revealed by isotope-edited Fourier transform infrared spectroscopy. *J. Am. Chem. Soc. 133*, 3808−3811.
(32) Tomita, M., Ifuku, K., Sato, F., and Noguchi, T. (2009) FTIR evidence that the PsbP extrinsic protein induces protein conformational changes around the oxygen-evolving Mn cluster in photosystem II. *Biochemistry 48*, 6318−6325.
(33) Noguchi, T., and Sugiura, M. (2002) FTIR detection of water reactions during the flash-induced S-state cycle of the photosynthetic water-oxidizing complex. *Biochemistry 41*, 15706−15712.
(34) Suzuki, H., Sugiura, M., and Noguchi, T. (2008) Monitoring water reactions during the S-state cycle of the photosynthetic water-oxidizing center: Detection of the DOD bending vibrations by means of Fourier transform infrared spectroscopy. *Biochemistry 47*, 11024−11030.
(35) Sugiura, M., and Inoue, Y. (1999) Highly purified thermo-stable oxygen-evolving photosystem II core complex from the thermophilic cyanobacterium *Synechococcus elongatus* having His-tagged CP43. *Plant Cell Physiol. 40*, 1219−1231.
(36) Noguchi, T., and Sugiura, M. (2002) Flash-induced FTIR difference spectra of the water oxidizing complex in moderately hydrated photosystem II core films: Effect of hydration extent on S-state transitions. *Biochemistry 41*, 2322−2330.
(37) Yuzawa, T., Kato, C., George, M. W., and Hamaguchi, H. (1994) Nanosecond time-resolved infrared-spectroscopy with a dispersive scanning spectrometer. *Appl. Spectrosc. 48*, 684−690.
(38) Noguchi, T., Tomo, T., and Kato, C. (2001) Triplet formation on a monomeric chlorophyll in the photosystem II reaction center as studied by time-resolved infrared spectroscopy. *Biochemistry 40*, 2176−2185.
(39) de Wijn, R., and van Gorkom, H. J. (2002) S-state dependence of the miss probability in Photosystem II. *Photosynth. Res. 72*, 217−222.
(40) Noguchi, T., and Sugiura, M. (2001) Flash-induced Fourier transform infrared detection of the structural changes during the S-state cycle of the oxygen-evolving complex in photosystem II. *Biochemistry 40*, 1497−1502.
(41) Hillier, W., and Babcock, G. T. (2001) S-state dependent Fourier transform infrared difference spectra for the photosystem II oxygen evolving complex. *Biochemistry 40*, 1503−1509.
(42) Noguchi, T., and Sugiura, M. (2003) Analysis of flash-induced FTIR difference spectra of the S-state cycle in the photosynthetic water-oxidizing complex by uniform ^{15}N and ^{13}C isotope labeling. *Biochemistry 42*, 6035−6042.
(43) Kimura, Y., Mizusawa, N., Ishii, A., Yamanari, T., and Ono, T. (2003) Changes of low-frequency vibrational modes induced by universal ^{15}N- and ^{13}C-isotope labeling in S_2/S_1 FTIR difference spectrum of oxygen-evolving complex. *Biochemistry 42*, 13170−13177.
(44) Zundel, G. (1988) Proton transfer in and proton polarizability of hydrogen bonds: IR and theoretical studies regarding mechanisms in biological systems. *J. Mol. Struct. 177*, 43−68.
(45) Berthomieu, C., Nabedryk, E., Mäntele, W., and Breton, J. (1990) Characterization by FTIR spectroscopy of the photoreduction of the primary quinone acceptor Q_A in photosystem II. *FEBS Lett. 269*, 363−367.
(46) Noguchi, T., Inoue, Y., and Tang, X.-S. (1999) Hydrogen bonding interaction between the primary quinone acceptor Q_A and a histidine side chain in photosystem II as revealed by Fourier transform infrared spectroscopy. *Biochemistry 38*, 399−403.

(47) Takano, A., Takahashi, R., Suzuki, H., and Noguchi, T. (2008) Herbicide effect on the hydrogen-bonding interaction of the primary quinone electron acceptor Q_A in photosystem II as studied by Fourier transform infrared spectroscopy. *Photosynth. Res. 98*, 159−167.
(48) Suzuki, H., Nagasaka, M., Sugiura, M., and Noguchi, T. (2005) Fourier transform infrared spectrum of the secondary quinone electron acceptor Q_B in photosystem II. *Biochemistry 44*, 11323−11328.
(49) Service, R. J., Hillier, W., and Debus, R. J. (2010) Evidence from FTIR difference spectroscopy of an extensive network of hydrogen bonds near the oxygen-evolving Mn_4Ca cluster of photosystem II Involving D1-Glu65, D2-Glu312, and D1-Glu329. *Biochemistry 49*, 6655−6669.
(50) Suzuki, H., Sugiura, M., and Noguchi, T. (2009) Monitoring proton release during photosynthetic water oxidation in photosystem II by means of isotope-edited infrared spectroscopy. *J. Am. Chem. Soc. 131*, 7849−7857.
(51) Barry, B. A., Cooper, I. B., De Riso, A., Brewer, S. H., Vu, D. M., and Dyer, R. B. (2006) Time-resolved vibrational spectroscopy detects protein-based intermediates in the photosynthetic oxygen-evolving cycle. *Proc. Natl. Acad. Sci. U.S.A. 103*, 7288−7291.
(52) Noguchi, T., Inoue, Y., and Tang, X.-S. (1999) Structure of a histidine ligand in the photosynthetic oxygen-evolving complex as studied by light-induced Fourier transform infrared difference spectroscopy. *Biochemistry 38*, 10187−10195.
(53) Kimura, Y., Mizusawa, N., Ishii, A., and Ono, T. (2005) FTIR detection of structural changes in a histidine ligand during S-state cycling of photosynthetic oxygen-evolving complex. *Biochemistry 44*, 16072−16078.
(54) Berthomieu, C., Hienerwadel, R., Boussac, A., Breton, J., and Diner, B. A. (1998) Hydrogen bonding of redox-active tyrosine Z of photosystem II probed by FTIR difference spectroscopy. *Biochemistry 37*, 10547−10554.
(55) Dekker, J. P., Plijter, J. J., Ouwehand, L., and van Gorkom, H. J. (1984) Kinetics of manganese redox transitions in the oxygen-evolving apparatus of photosynthesis. *Biochim. Biophys. Acta 767*, 176−179.
(56) Renger, G., and Weiss, W. (1986) Studies on the nature of the water-oxidizing enzyme. III. Spectral characterization of the intermediary redox states in the water-oxidizing enzyme system Y. *Biochim. Biophys. Acta 850*, 184−196.
(57) Saygin, Ö., and Witt, H. T. (1987) Optical characterization of intermediates in the water-splitting enzyme-system of photosynthesis: Possible states and configurations of manganese and water. *Biochim. Biophys. Acta 893*, 452−469.
(58) Babcock, G. T., Blankenship, R. E., and Sauer, K. (1976) Reaction kinetics for positive charge accumulation on water side of chloroplast photosystem II. *FEBS Lett. 61*, 286−289.
(59) Razeghifard, M. R., and Pace, R. J. (1997) Electron paramagnetic resonance kinetic studies of the S states in spinach PSII membranes. *Biochim. Biophys. Acta 1322*, 141−150.
(60) Christen, G., Reifarth, F., and Renger, G. (1998) On the origin of the '35-μs kinetics' of $P680^{+\bullet}$ reduction in photosystem II with an intact water oxidising complex. *FEBS Lett. 429*, 49−52.
(61) Schilstra, M. J., Rappaport, F., Nugent, J. H. A., Barnett, C. J., and Klug, D. R. (1998) Proton/hydrogen transfer affects the S-state-dependent microsecond phases of $P680^+$ reduction during water splitting. *Biochemistry 37*, 3974−3981.
(62) Förster, V., and Junge, W. (1985) Stoichiometry and kinetics of proton release upon photosynthetic water oxidation. *Photochem. Photobiol. 41*, 183−190.
(63) Schlodder, E., and Witt, H. T. (1999) Stoichiometry of proton release from the catalytic center in photosynthetic water oxidation: Reexamination by a glass electrode study at pH 5.5−7.2. *J. Biol. Chem. 274*, 30387−30392.